CHEMISTRY
AN ASIAN JOURNAL
www.chemasianj.org

Accepted Article

Title: Influence of alkanolamine plasmas on poly(ethylene terephthalate) fibrous biomaterial constructs

Authors: Bernabe S Tucker, Gerardo Hernández Moreno, Patrick T.J. Hwang, Ho-Wook Jun, and Vinoy Thomas

To be cited as: *Chem. Asian J.* **2024**, e202400796

Link to VoR: https://doi.org/10.1002/asia.202400796

A Journal of

ACES Asian Chemical Editorial Society

WILEY VCH

10.1002/asia.202400796

Influence of Alkanolamine Plasmas on Poly(ethylene terephthalate) Fibro-porous Biomaterial Constructs

Bernabe S. Tucker[1], Gerardo Hernandez-Moreno[1], Patrick T. J. Hwang[2], Ho-Wook Jun[2], and Vinoy Thomas[1,2,3*]

[1] Department of Mechanical and Materials Engineering, University of Alabama at Birmingham, AL 35294, USA.
[2] Department of Biomedical Engineering, University of Alabama at Birmingham, AL 35294, USA
3. Center for Nanoscale Materials and Biointegration, University of Alabama at Birmingham, USA.
* For Correspondence : Dr. Vinoy Thomas, vthomas@uab.edu

Abstract

The development of fibrous polymer scaffolds is highly valuable for applications in tissue engineering. Furthermore, there is an extensive body of literature for chemical methods to produce scaffolds that release nitric oxide. However, these methods often use harsh chemistries and leave behind bulk waste. Alkanolamine low-temperature plasma (LTP) is unexplored and single-step processing to form nitric oxide (NO) releasing constructs is highly desirable. The major question addressed is whether it is possible to achieve single-step processing of spun polyester with alkanolamine plasma to achieve nitric oxide releasing capabilities. Herein we report the experiments, processes, and data that support the claim that it is indeed possible to produce such a bio-functional material for potential biomedical applications, especially in cardiovascular implants. Among the tested alkanolamines, monoethylamine (MEA) plasma treated biomaterial outperformed in comparison with diethanolamine (DEA) and triethanolamine (TEA) in terms of NO release and cellular response.

Introduction

Small-caliber vascular grafts (< 6 mm inner diameter) are highly desirable and currently unavailable in the vascular graft market. The incidence of vascular graft failure in the small-diameter regime is a due to a combination of factors. These include: the lack of facile, rapid and confluent development of an endothelial cell layer, mismatch of properties between the host tissue and the graft, and the aggregation/activation of platelets which can lead to thrombosis. It is well documented that nitric oxide (NO) and nitroxyl (HNO) releasing compounds are potent vasodilators, which are often prescribed during treatment for cardiovascular disease (CVD) patients. There is vast literature regarding the importance and pathways associated with both endogenous and exogenous NO and especially for CVD pathologies [1]. An example of a prodrug for NO is nitroglycerin which is often prescribed to patients suffering from chest pains. Compounds with the moiety S-nitrosothiol represent one of the largest and most well-known classes of chemical NO donors for research purposes. Thus, nitric oxide releasing scaffolds are established to be a beneficial target for functional material design. To date, there has been little to no exploration of organic nitrogenous low-temperature plasmas (LTP) for introducing NO/HNO functionalization. However, the general idea for NO-releasing scaffolds and plasma activation appears to be generating much interest in recent reports. NO releasing peptide amphiphilic nanomatrix has been developed by wet-chemical methods and utilized for nanostructured scaffold fabrication for various applications [2]. Electrospinning has been widely used for making seamless tubes of any diameter and length for experimental vascular grafts with mimicking nanofiber features of protein matrices [3-5]. We have recently fabricated small diameter kink-free tubular graft by combining electrospinning and 3D- printing methods [6]. Low temperature plasma (LTP) has been attracted much attention for surface engineering biomaterials without affecting their bulk mechanical

properties [7-9]. Specifically for blood contacting vascular materials such as e-PTFE, plasma polymerization using organosilane plasma has shown favorable blood compatibility by increased growth of endothelial cells and reduced number of adhered platelets under in vitro conditions [10]. The focus of this study is to use nitrogenous, organic LTP to directly synthesize NO-releasing layers on poly(ethylene terephthalate) (PET) for the following reasons: (1) PET represents an established material toward the specific tissue engineering application of synthetic vascular grafts. (2) PET surfaces can be rendered more hydrophilic with LTP processing. (3) NO-releasing scaffolds offer functional materials for CVD tissue engineering.

In recent years there have been several experimental reports showing a convergence of the ideas of NO-releasing surfaces and LTP techniques to modify polymers such as PET [11-14]. But, a gap in knowledge exists in the regime of organic vapor plasmas and how these can produce functional materials that release NO from direct synthesis on the surface. Current literature still reports the use multi-step processes [11,12,14]. This work aims to address this gap through an experimental approach that employs LTP processing and fibrous polymer constructs. This combination is to produce functional materials that release NO from single-step processing.

The scope of this work is limited to investigating the plasma/surface interactions and their post-processing behavior. Mechanisms of NO bio-pathways and live tissue engineering shall remain beyond the direct scope although preliminary *in vitro* data is provided as proof-of-concept. Previously, this lab has reported electrospinning and LTP techniques toward biomaterials applications [15, 16]. One important lesson learned was the propensity for LTP treated surfaces to age rapidly. In LTP where the working gas is air it is possible to achieve nitrogen functionalization on the surface, however, it is easily lost during the aging process. In this current approach organic precursors are employed to provide a more resilient surface processing. It is quite

common and desirable to introduce nitrogen to surfaces and several recent methodologies advice the use of different precursors toward surface amination ranging from ammonia to large organic amines [17-19]. By contrast alcohol-based LTP are rarer and typically procedures are tuned for alcohol decomposition [20-24]. Herein, three precursors are chosen that combine both alcohol and amine functionality, hence, they are termed alkanolamines. They are 2-aminoethan-1-ol or monoethanolamine (MEA, 2,2′-azanediyldi(ethan-1-ol) or diethanolamine (DEA), and2,2′,2″-nitrilotri(ethan-1-ol), or triethanolamine (TEA). The given supplementary information **S1 and S2** depicts the chemical structures and molecular orbital structures of these molecules showing both the amine and alcohol functionality. Regarding the molecular orbital structures, the lowest occupied molecular orbital (LUMO) of MEA is asymmetrical with respect to the distribution around the molecule which is not surprising considering each side is chemically different. The LUMO of DEA is more symmetrical since each end is the same consisting of hydroxyl groups and the secondary amine functionality in the center of the molecule. Further, the LUMO of TEA resembles that of DEA but the third alcohol branch has a smaller orbital distribution. The energies of both the LUMO and highest occupied molecular orbital (HOMO) were also calculated, and these results shown in **S2**. These precursors were subjected to non-magnetized LTP conditions at medium pressures and various exposure times. The influence of these plasmas on electrospun mats of PET fibers are characterized, documented and reported following.

Experimental Materials and Methods

Electrospinning

Electrospinning was carried out with a custom-built apparatus described in some previous reporting from our lab [15]. Briefly, a working solution is pumped at a constant rate through a

needle, across a set distance, with a multi-kilovolt electric potential relative to a grounded collector, and fibers are obtained which can be collected in mats. First, three different concentrations were selected at 5%, 10%, and 20% w/v based on the solubility of PET in the solvent 1,1,1,3,3,3-hexafluoropropan-2-ol, also known as hexafluoroisopropanol or HFIP. Distances of 10, 15, 20, and 30 cm of needle (25 G, BD syringe) to collector were tested and three potentials of 5, 10, and 20 kV with the needle positive and collector grounded were also tested. It was found, consistent with expectations, that low-viscosity, low-voltage conditions led generally to electrospray mode. In electrospray mode the polymer forms particles rather than fibers. Under moderate conditions a variety of mixed modes, with both fibers and beads, were observed. Finally, under high viscosity and high voltage conditions pristine, bead-free fibers where observed. An arbitrary choice was used and set constant for all subsequent experiments. A rotating cylindrical collector (hollow aluminum cylinder, 5 cm outer diameter, 150 RPM) was used to obtain large amounts of fiber mats for experiments. The working solution was 20% w/v and was pumped at 1.0 mL/h through a 25 G needle and the needle was given lateral motion of 150 mm displacement at a rate of 25 mm/s with a potential of 16 kV (needle positive, collector ground). The Supplementary Information, **S3** depicts some images from the optimization experiments.

Plasma Processing and Optical Spectroscopy

Plasma conditions were accessed with a Harrick PDC-001 plasma cleaner (Harrick Plasma, NY, USA). The 45 W setting was employed, and no feed gas used. The organic precursors were added in 100 µL increments per run with the use of a 96-well plate which also served as a sample holder. During evacuation with a pump the pressure was recorded during processing (Supplementary information **S4 and S5).** Only the evaporation rate of the precursor controlled the mass flow in the system. The For optical emission measurements an Ocean Optics USB

4000 spectrometer (Florida, USA) was employed by tilting the optical slit toward the window of the Harrick chamber by clamping in a ring stand; positioning was marked with tape to repeat the location. The OceanSuite software was used to capture live spectra with a 500 ms integration time, 4 scan averaging, value of 2 for the boxcar average width, and electronic dark correction and nonlinear correction added. The live output was subtracted from a dark spectrum to correct for baseline. The spectrometer was uncooled and used at ambient conditions. Immediately after processing some samples were taken for temperature measurements with a FLIR C2 imager (Teledyne FLIR LLC, Oregon, USA). These images were taken against a cutting mat as a background with the optical image overlaid for additional detail (**S 6**).

FT-IR Functional Group Analysis

For bulk chemical information Fourier-transform infrared (FTIR) spectroscopy was employed using a Nicolet 4700 FTIR instrument. Small discs of material were cut with a biopsy punch and pressed onto the attenuated total internal reflection (ATR) diamond window. The spectra were captured with 32 scans at 2 cm^{-1} resolution from the range 500 – 4000 cm^{-1}. ATR corrections were applied along with automatic baseline and smoothing in the OMNIC software supplied with the instrument.

Contact Angle Experiment

For the aging and surface analysis study a custom-built contact angle goniometer was constructed. It used a machined aluminum optical table (4” x 4”) that served as the sample stage. The measurements were taken with a Canon TV zoom lens 12 - 75 mm with the shutter at f/16 and a +10-macro attachment added. The 5 µL drop of DI water was added with a calibrated syringe and images taken by CCD sensor attached to a 2012 MacBook Pro running USB Pluggable Digital Viewer microscope software. Angles were taken from the angle tool in ImageJ software.

Aging was carried out by keeping samples at various conditions in the freezer, benchtop, and a warming plate. The samples all were kept inside 12-well plates to keep out contamination. Further, since the electrospun samples were too porous to measure, samples of mylar were used as a stand-in and subjected to the sample treatments with LTP as the electrospun sheets.

Thermal Characterization (DSC)

Thermal characterization was carried out with a Q-600 differential scanning calorimeter (DSC) from TA Instruments. For DSC small samples were carefully cut with a biopsy punch and loaded into hermetic aluminum pans available from TA. The runs were set from RT to 300 °C at 10 °C/min heating rate with 50 mL/min dry nitrogen flow. For the analysis was done in TA Universal Analysis Software.

Mechanical Characterization (Tensile test)

Mechanical characterization by tensile method was conducted with a RSA-G2 dynamic mechanical analyzer (DMA) by TA instruments with the tensile fixture attached and samples of material cut carefully into tensile bars with an average thickness of 0.2mm, a 20 mm gauge length, 5 mm width, and with 5 mm of tab to clamp on each side. The tensile specimens were subjected to a linear rate of 0.5 mm/s and stress/strain data collected at 5 pts/s at RT.

Bovine Serum Albumin-fluorescein isothiocyanate modified (BSA-FITC) assay

The protein adsorption assay was conducted by taking biopsy punch samples of the materials and soaking them in 1.0 mg/mL solutions of BSA-FITC in 1X PBS buffer (7.4 pH) at RT for 12 h. Subsequently, the samples were rinsed for 12 h at RT in 1X PBS and the resultant solutions analyzed in a gel-doc imaging system with a Canon Rebel SLT camera equipped with a 28 – 80 mm lens set to 50 mm with f/11 at 2.5 s shutter speed or adjusted according to the onboard

light meter. The images were processed in ImageJ and data collected from the output tables for line profiles to measure the intensity as a function of fluorescent intensity.

Fibroblast cell culture on electrospun sheets and MTT assay

Human fibroblast cells were obtained and cultured in Growth media. Cells were grown to 70%–80% confluence at normal culture conditions (37°C, 95% humidity, 5% CO2) before being seeded onto the electrospun sheets.

Samples of biopsy punched materials were loaded into well plates and seeded at 300k cells/well with growth media and incubated under typically culture conditions. MTT assay was performed as per kit instructions and reported as absorbance values for each well.

X-ray photoelectron spectroscopy (XPS) surface analysis

Surface chemistries for the optimization study were collected with a Phi Versaprobe XPS system and used in accordance with standard procedures in previously reported literature from the lab [15-17].

Nitric oxide (NO) release measurements

A standard Griess assay procedure adopted from Promega was conducted with sourced components and measured with a BioRad 580 absorbance plate reader. Samples were incubated at various time points to elucidate the released NO profiles in 1X PBS at RT. 100 µL of test sample was added to 100 µL of Griess reagent solution and incubated for 10 min at RT to an end point measured with dual-wavelength mode of 415 nm monitor and 530 nm measure filters on the plate reader. Samples were replicated in triplicate.

Endothelial Cell Culture on Fibrous Sheets and MTS assay

Human aortic endothelial cells (HAECs) were obtained from Lonza, Inc and cultured in Endothelial Growth Media (EGM-2 BulletKit; Lonza, Walkersville, MD). Cells were grown to

70%–80% confluence at normal culture conditions (37°C, 95% humidity, 5% CO2) before being seeded onto electrospun sheets.

Samples for quantitative analysis of cell proliferation were prepared by cutting electrospun sheets into circles with a diameter of 6.4 mm. These sheets were then sterilized with UV light for 3 hours before being loaded into 96 well plates. 9,000 HAEC cells were then seeded onto each sheet along with 200 µL of media. The cells were cultured at 37 ºC for 3 days. Next, an MTS [3-(4,5-dimethylthiazol-2-yl)−5-(3-carboxymethoxyphenyl)−2-(4sulfophenyl)-2H-tetrazolium] assay (CellTiter 96 solution, Promega Co.) was performed to measure HAEC proliferation on the sheets. Cell proliferation on each treatment condition on the electrospun sheets was measured with sample size n=5.

LIVE/DEAD Assay and Imaging for Fibrous Sheets

Electrospun fibrous sheets of varying treatments were cut into circles with a diameter of 9.5mm and UV sterilized for 3 hours. After placing the cut sheets into 48 well plates, 25,000 HAEC cells along with 400 µL of media were seeded onto each sheet. The cells were cultured for 3 days at 37 0C after which living cells were stained by using a Live/Dead Viability (Molecular Probes Inc., OR). These living cells were then visualized using a Nikon fluorescent microscope and ImageJ software.

The sample preparation procedure for the LIVE/DEAD assay was repeated for cell imaging. 25,000 HAEC cells along with 400 µL of media were seeded onto each electrospun PCL sheet after being placed into 48 well plates. After culturing the cells at 37 0C for 3 days, the samples were fixed with paraformaldehyde. The electrospun sheets were imaged using a Quanta 650 FEG (FEI Co.) with an accelerating voltage of 10 kV. Also, they were imaged with a Nikon fluorescent microscope

10.1002/asia.202400796

Results and Discussion

The major questions that were tested included whether nitric oxide could be released by the LTP treated materials and whether the choice of precursor had an effect. Initially, it was suspected that the MEA would have the greatest potential of working compared to the DEA and TEA. First, the MEA molecule is smaller and the nitrogen is primary, thus, less hindered than in DEA or TEA. Next, as shown in **S2** the LUMO is quite asymmetrical in MEA especially with respect to the location near the nitrogen. We surmise that this asymmetry is the source of a diversity of LTP products of which some are capable of degrading into nitric oxide in aqueous conditions that we observed as a nitrite end product detectable by the Griess assay.

Optical emission during plasma processing

In the initial period, once the MEA plasma is activated, it has the characteristics of an air plasma. This is due to the residual air in the chamber and conveniently acts as an oxidative plasma to activate the surfaces of the materials. Next, as more precursor is evaporated several striking features are noted. The emergence of a strong hydrogen-alpha line is observed along with a possible hydrogen-Fulcher band. Also, nitrogen molecular lines are seen. There are strong lines associated with carbon monoxide (CO) in the 400 – 600 nm range along with a broad background that overlaps with the C_2 Swan bands. This indicates various molecular fragments in the plasma resulting from the breakdown and ionization of the parent precursor molecules. These species can then land, attach, and react with other species forming a variety of surface products rich in nitrogen, oxygen, and carbon containing functionality. Presumably, there is also a flux of energetic electrons that can contribute to surface reactions, surface radicals and rearrangements.

However, due to the short lifetimes and hinderance from the PET polymeric chains their influence does not affect the inner layers of the fibrous materials. **Figure 1** summarizes the OES data for the MEA plasmas.

In the initial period, once the DEA plasma is activated, it has the characteristics of an air plasma like the behavior of the MEA plasma. Likewise, this is also due to the residual air in the chamber and conveniently acts as an oxidative plasma to activate the surfaces of the materials similar to the MEA plasma. Next, however, as more precursor is evaporated several differing features are noted. The emergence of a strong hydrogen-alpha line is observed along with a possible hydrogen-Fulcher band and is of much greater intensity that in the MEA plasma. This could be the result of since more hydroxyl groups are present and the strength of the alkoxide ion leading to ease of hydrogen cleavage and excitation to account for the higher H-alpha output. Also, nitrogen molecular lines are seen and stronger that in the MEA. There are weak lines associated with carbon monoxide (CO) in the 400 – 600 nm range along with a broad but more subtle background that overlaps with the C_2 Swan bands, although not to the degree found in MEA plasma. There would be a different diversity of products from the DEA-LTP that could land on the PET fibers. Thus, the resulting treated material would behave differently from the MEA-LTP. **Figure 2** summarizes the OES data for the DEA plasmas.

In the initial period, once the TEA plasma is activated, it has the characteristics of an air plasma like the behavior of the MEA or DEA plasma. Likewise, this is also due to the residual air in the chamber and conveniently acts as an oxidative plasma to activate the surfaces of the materials similar to the other plasmas. Next, however, as more precursor is evaporated several differing features from the MEA-LTP but similar to the DEA-LTP are noted. There is still the emergence of a strong hydrogen-alpha line is observed along with a possible hydrogen-Fulcher

band and is of much greater intensity that in the MEA plasma but similar to the DEA plasma. This could be the result of since even more hydroxyl groups are present that for MEA/DEA. Also, nitrogen molecular lines are seen and stronger that in the MEA similar to the DEA. There are weak lines associated with carbon monoxide (CO) in the 400 – 600 nm range along with a broad background that overlaps with the C_2 Swan bands, although not to the degree found in MEA plasma and more similar to the DEA. There would be a different diversity of products from the TEA-LTP that could land on the PET fibers. Thus, the resulting treated material would behave differently from the MEA-LTP and likely behave more like DEA-LTP treated material. **Figure 3** summarizes the OES data for the TEA plasmas.

Contact Angle Wettability Studies

The wetting behavior associated with plasma treated samples is desirable for biomaterial type applications. However, an unfortunate effect is the tendency to have hydrophobic recovery in the days post treatment. This is quite well known and still unavoidable. In the contact angle data, there are time points of 1, 3, 5, and 14 days along with various temperature conditions of 0 °C, RT, and body temperature to gauge the effects of temperature on aging.

It was found that the MEA treated samples had the most hydrophilic behavior post LTP treatment and the data is shown in **Figure 4**. In fact, some samples were difficult to measure since the drop spread out so broadly. Overall, the longer the treatment time the more the hydrophilic behavior dominated the earlier time points or 1 and 3 days. However, by 5 days hydrophobic recovery had set in. Since the OES data indicated a diversity of potential products that most likely are polar since oxygen and nitrogen might easily attach these data taken together support the idea of a greater array of surface products are the result of a small, orbitally asymmetric precursor, than for the larger more symmetric molecules.

It was found that the DEA treated samples had less hydrophilic behavior post LTP treatment compared to the MEA treated samples and the data is shown in **Figure 5**. Overall, the treatment time did not have as dramatic of an effect as the MEA-LTP samples. Hydrophobic recovery had set in earlier around the 3-day time frame and the aging behavior was more subtle than MEA. Since the OES data indicated a different, more hydrogen dominated plasma which could provide a more reducing environment and with more alkyl groups available, the notion of a less hydrophilic surface is substantiated.

It was found that the TEA treated samples had less hydrophilic behavior post-LTP treatment compared to the MEA treated samples and similar to the DEA treated samples and the data is shown in **Figure 6**. Overall, the treatment time did not have as dramatic of an effect as the MEA-LTP samples and more closely resembled the DEA treated samples. Hydrophobic recovery had set in earlier around the 3-day time frame and the aging behavior was more subtle than MEA and more closely matched the DEA. Since the OES data indicated a different, more hydrogen dominated plasma which could provide a more reducing environment and with even more alkyl groups available similar to the DEA plasma, the similar noted behavior is expected.

Overall, the major factor in aging was the time. The most the samples could retain hydrophilic behavior was 3 days before succumbing to the effects of ageing. The temperature did not have as dramatic of an effect as did the time. Thus, for application purposes these materials must be used rapidly to maintain their functionality. The stability of surface functionalities is still a challenge for long-term applications of plasma modified materials. However, the plasma enhanced coating by polymerization may alleviate this issue on aging stability [10].

Bulk Chemical Functional Group Characterization

The FTIR spectra indicated various functional groups such as alkyl, carbonyl, and aromatic which are present in the parent PET polymer. Thus, this technique was unable to distinguish among the untreated or LTP treated samples. **Figure 7** provides a summary of the data. Thus, it can be concluded that the chemical effects were relegated to the surface and did not substantially alter the bulk chemical properties.

Thermal Properties by Differential Scanning Calorimetry (DSC)

The DSC experiments indicate that the thermal properties remained largely unchanged. The large broad peaks for both the cold crystallization and melt were roughly located at the same temperature ranges for each of the samples both treated and untreated. Although, there seemed to be a dramatic reduction in glass transition that was associated with the LTP treated of DEA and TEA might indicated that some of the LTP products could be acting a plasticizer. Although, there was doubt since the deflection of the thermogram was subtle and the software might not be as sensitive to such a small deflection. **Table 1** summarizes the findings from DSC analysis including the calculated enthalpies of the melt and cold crystallization peaks.

Tensile Mechanical Properties

In general, the stress/strain behavior of the fibers showed sharp initial linear regions from which the Young's moduli were extracted. After yield, nearly perfect plastic deformation behavior is noted, and a rapid decline of the stress curve is seen after fracture. Residual fibers still attached account for the non-zero values after the breaks. The deformation behavior is governed by rearrangement of the fibers and is very noisy. Thus, the statistically significant differences might be due to bonding effects between the fibers that accounts for the different mechanical properties. However, since the data are quite noisy it is not conclusive. Further, this type of noise has been encountered by previous attempts in the lab to elucidate the true mechanical properties of

these fibers. The tensile data are provided in **Figure 8**. The inherently random nature of the fibrous nature would be expected to contribute to these effects.

Protein Adsorption Tests

The protein bovine serum albumin (BSA) was chosen as a model protein to mimic the potential for absorbing proteins in a biologically relevant setup. BSA-fluorescein isothiocyanate (BSA-FITC) is a well-known BSA modification that allows quantification by fluorescence. The overall trend was that the LTP treated samples adsorbed more protein than the control with DEA samples adsorbing the most and TEA adsorbing the least with MEA intermediate among LTP treated samples. The exposure times did not seem to make as dramatic of a difference as did whether or not the samples were exposed to plasma. From this data it can be surmised that all the plasma treated samples may behave well toward biological situations. These data are shown in **Figure 9**. The adsorption of BSA is quite complex as there are dozens of residues with both polar and non-polar qualities which could influence the tendencies toward surface adsorptions. However, it is clearly seen that the control fibers are avoidant toward adsorption and this effect can be attributed to their very hydrophobic character as demonstrated with the contact angle experiment.

Fibroblast Cytocompatibility Assay

The BSA-FITC assay demonstrated that the time point of LTP exposure was not very important toward protein adsorption. Therefore, it was decided to use only the 10-minute exposure time for the MEA, DEA, and TEA LTP treated samples and to compare this to the plate grown cells and untreated samples using the well-known MTT assay reported as absorbance values in **Figure 10**. Overall, the electrospun PET material is very cytocompatible with fibroblast cells and the LTP treated samples exhibited excellent compatibility on par with the tissue culture plate.

The control untreated samples were significantly different from the plated cells whereas the LTP treated samples were not. Thus, it can be concluded that any of the LTP treated samples would be excellent for using in fibroblast culture applications.

Surface Chemistry Investigation and In vitro Data

The question of whether these PET fiber mats could release nitric oxide was tested using the well-known Greiss assay which measures nitrite as the end product of a nitric oxide releasing situation. The reaction produces an intensely colored compound as it shown in **Figure 11**. The MEA treated samples seemed to have the highest response with DEA showing a little response and the TEA showing no response. Thus, we decided to further investigate the degree of release for MEA-LTP treated fibers as a NO-releasing functional material. The dual-filter method was employed to eliminate the effect of the potential side products from the 1 min MEA samples. To understand what might be occurring, though, an investigation with XPS was employed to track the surface nitrogen to oxygen ratio and see if it was possible to tune the surface with plasma exposure time. The XPS results show 10 min exposure to be the ideal time point since the system achieve a 1:1 N/O ratio. The XPS data are shown in **Figure 12**.

Since it was not observed that N/O ratio goes above 1:1 as nitrogen appears to reach a maximum surface concentration around 10 min, this time point was chosen for the endothelial cell test. But first, it was desirable to highlight the quantitative release profiles with a more thorough NO assay and the data are shown for cumulative release in **Figure 13**.

The cumulative release profiles show that the time frame for release of NO from the surface occurs between 10 min and 100 min and further flux is negligible after 100 min for all sam-

ples. Furthermore, it seems that the 10 mins treatment time with the 1:1 N/O surface concentration has the greatest amount of NO released. The 10 min MEA sample was compared to the control untreated sample and well plate in an endothelial cell study.

The results of the endothelial cell study were lackluster when comparing the samples to the well plate and are shown in **Figure 14**. Although, the geometry of the test samples may not be optimized since endothelial cells are quite sensitive and difficult to culture. The positive increase in MEA treated sample compared to the control sample, however, is encouraging that the LTP treatment does help. However, the SEM micrographs (**Figure 15)** apparently indicate spreading of the endothelial cells showing strong affinity for the LTP treated fibers, whereas they do not for the control fibers. Furthermore, the live/dead fluorescent micrographs show the field of view is vibrant with many more endothelial cells in the treated samples vs. the control. This seems to indicate that the LTP treatment indeed made a functional surface on the otherwise inert, hydrophobic, unmodified electrospun PET fibers. NO-releasing fibro-porous constructs could be useful for wound healing applications [25,26] when combined with anti-bacterial properties as recently published plasma electroless reduction process [27,28]. However, sustained release of NO and functional dosage in dynamic environment is still needed to be investigated to warrant application for vascular graft or tissue scaffolds.

Conclusions

There is strong support for the hypothesis that the LTP treatments can indeed produce a functional material that releases nitric oxide and the measured amounts are in the micromolar range over timescales of 100 minutes. The data show that LTP treatment has a minimal effect on

the bulk properties and that most of the changes are on the surface. Thus, engineering of a macro-construct can be separated from the surface engineering. In an application such as a vascular graft where both fibroblast and endothelial cells would be present this material system provides an attractive candidate for future studies. In short, MEA plasma treated biomaterial outperformed in comparison with DEA and TEA in terms of NO formation/release.

Acknowledgments

The authors acknowledge the support from the programmatic grants U.S. NSF EPSCoR OIA-2148653, US DoEd. GAANN Grant No. P200A180001 and Alabama Department of Economic and Community Affairs (ADECA) grant 1ARDEF 23 01 for major funding toward this study. The authors also acknowledge Mr. Halloran at UAB and to Keyence Corporation for images (not shown) during the optimization of fibrous mats. The opinions presented herein do not necessary reflect the official positions of any US funding agency.

References

1. F. Doctorovich, P. J. Farmer, M. A. Marti, (Eds.), The Chemistry and Biology of Nitroxyl (HNO), 2017, Elsevier, Amsterdam, Netherlands, p 15-387.
2. P. Hwang CM. Shin, JA Sherwood, DH Kim, VM. Vijayan, KC. Josyula, RC. Millican, D. Ho, BC. Bott, V. Thomas, CH. Choi, SH. Oh, DW. Kim, HW. Jun, A multitargeting bionanomatrix coating to reduce capsular contracture development on silicone implants, Biomaterials Research, 2023, 27, 34.

3. HN. Patel, YK. Vohra, RK. Singh, V. Thomas, HuBiogel incorporated fibro-porous hybrid nanometric graft for vascular tissue interfaces, Mater. Today Chem, 2020, 17, 100323.

4. V. Thomas, X. Zhang, YK. Vohra, A biomimetic tubular scaffold with spatially designed nanofibers of potential protein/PDS bioblends, Biotechnol. Bioengineering, 2009, 104, 1025.

5. X. Zhang, Y. Xu. V. Thomas, SL. Bellis, YK. Vohra, Engineering an antiplatelet adhesion layer on an electrospun scaffold using porcine endothelial progenitor cells, J. Biomed. Mater res, 2011, 97, 145.

6. KR. Adhikari, J Zimmerman, PD. Dimble, BS. Tucker, V. Thomas, Kink free electrospun PET/PU based vascular graft with 3D printed additive manufacturing reinforcement, J Mater. Res. 2021, 36, 4013.

7. BS Tucker, S Aliakbarshirazi, VM. Vijayan, M. Thukkaram, N De Geyter, V. Thomas, Nonthermal plasma processing for nanostructured biomaterials and tissue scaffolds: a mini review, Curr. Opinion in Biomed. Eng., 2021, 17, 100259.

8. C. Kathik, S. Rajalakshmi, S. Thomas, V. Thomas, Intelligent polymeric biomaterials surface driven by plasma processing, Curr. Opinion in Biomed. Eng., 2023, 26, 100440.

9. C. Karthik, SC. Sarngadharan, V. Thomas, Low temperature plasma techniques in biomedical applications and therapeutics: An overview.

10. VM. Vijayan, BS. Tucker, PA. Baker YK. Vohra, V. Thomas, Non-equilibrium organosilane plasma polymerization for modulating the surface of PTFE towards potential blood contact applications. J. Mater. Chem 2020, 8(14), 2825.

11. R. Simon-Walker, R. Romero, J. M. Staver, Y. Zang, M. M. Reynolds, K. C. Popat, M. J. Kipper, Glycocalyx-Inspired Nitric Oxide-Releasing Surfaces Reduce Platelet Adhesion and Acitvation on Titanium, ACS Biomater. Sci. Eng. 2017, 3, 1, 68–77.

12. H. Qiu, P. Qi, J. Liu, Y. Yang, X. Tan, Y. Xiao, M. F. Maitz, N. Huang, Z. Yang, Biomimetic engineering endothelium-like coating on cardiovascular stent through heparin and nitric oxide-generating compound synergistic modification strategy, Biomaterials, 2019, 207, 10-22.

13. F. Rezaei, M. D. Dickey, M. Bourham, P. J. Hauser, Surface modification of PET film via a large area atmospheric pressure plasma: An optical analysis of the plasma and surface characterization of the polymer film, Surf. and Coatings. Technol., 2017, 309, 371-381.

14. M. N. Mann, B. H. Neufeld, M. J. Hawker, A. Pegalajar-Jurado, L. N. Paricio, Plasma-modified nitric oxide-releasing polymer films exhibit time-delayed 8-log reduction in growth of bacteria, Biointerfaces, 2016, 11, 031005.

15. B. S. Tucker, P. A. Baker, K. G. Xu, Y. K. Vohra, V. Thomas, Atmospheric pressure plasma jet: A facile method to modify the intimal surface of polymeric tubular conduits, Journal of Vacuum Science and Technology A, 2018, 36, 04F404.

16. B. S. Tucker, V. M. Vijayan, Y. K. Vohra, V. Thomas, Novel magneto-plasma processing for enhanced modification of electrospun biomaterials, Materials Letters, 2019, 250, 96-98.

17. K. V. Chan, M. Asadian, I. Onyshchenko, H. Declercq, R. Morent, N. De Geyter, Biocompatibility of Cyclopropylamine-Based Plasma Polymers Deposited at Sub-Atmospheric Pressure on Poly (ε-caprolactone) Nanofiber Meshes, Nanomaterials, 2019, 9, 9, 1215.

18. M. Mahmoudifard, M. Soleimani, M. Vossoughi, Ammonia plasma-treated electrospun polyacrylonitryle nanofibrous membrane: the robust substrate for protein immobilization through glutaraldhyde coupling chemistry for biosensor application, Scientific Reports, 2017, 7, 9441.

19. H. Savoji, A. Hadjizadeh, M. Marie, A. Ajji, M. R. Wertheimer, S. Lerouge, Electrospun Nanofiber Scaffolds and Plasma Polymerization: A Promising Combination Towards Complete, Stable Endothelial Lining for Vascular Grafts, Macromolecular Bioscience, 2014, 14, 8, 1084-1095.

20. L. Hui-qing, Z. Ji-jun, Z. Yue-ping, L. Chang-jun, Novel Plasma Methanol Decomposition to Hydrogen Using Corona Discharges, Chemistry Letters, 2004, 33, 6, 744-745.

21. M. C. Hsiao, B. T. Merritt, B. M. Penetrante, G. E. Vogtlin, P. H. Wallman, Plasma-assisted decomposition of methanol and trichloroethylene in atmospheric pressure air streams by electrical discharge processing, Journal of Applied Physics, 1995, 78, 5, 3451.

22. R. Rincon, A. Marina, J. Munoz, C. Melero, M. D. Calzada, Experimental research on ethanol-chemistry decomposition routes in a microwave plasma torch for hydrogen production, Chemical Engineering Journal, 2016, 284, 1117-1126.

23. C. L. Rinsch, X. Chen, V. Panchalingam, R. C. Eberhart, J. H. Wang, R. B. Timmons, Pulsed Radio Frequency Plasma Polymerization of Allyl Alcohol: Controlled Deposition of Surface Hydroxyl Groups, Langmuir, 1996, 12, 12, 2995-3002.

24. M. Jimenez, R. Rincon, A. Marinas, M. D. Calzada, Hydrogen production from ethanol decomposition by a microwave plasma: Influence of the plasma gas flow, International Journal of Hydrogen Energy, 2013, 38, 21, 8708-8719.

25. J. Durao, N. Vale, S. Gomes, P. Gomes, C. C. Barrias, L. Gales. Nitric oxide release from antimicrobial peptide hydrogels for wound healing, Biomolecuales, 2019, 9, 4. doi: 10.3390/biom9010004

26. G. Tavares, P. Alves, P. Simoes, Recent advances in hydrogel mediated nitric oxide delivery systems targeted for wound healing applications. Pharmaceuticals 2022, 14, 1377.

27. V. M. Vijayan, M. Walker, R. R. Pillai, G. Hernandez-Moreno, Y. K. Vohra, J. J. Morris, V. Thomas, Plasma electroless reduction: a green process for designing metallic nanostructure interfaces onto polymeric surfaces and 3D scaffolds, ACS. Appli. Mater. Interfaces, 2022, 14, 25065.

28. G. Hernandez-Moreno, V. M. Vijayan, B. A. Halloran, N. Ambalavanan, A. L. Hernandez-Nichols, J. P. Bradford, R. R. Pillai, V. Thomas, A plasma-3D print combined in vitro platform with implications for reliable materio-biological screening, J. Mater. Chem B, 2024, 12, 6654.

10.1002/asia.202400796

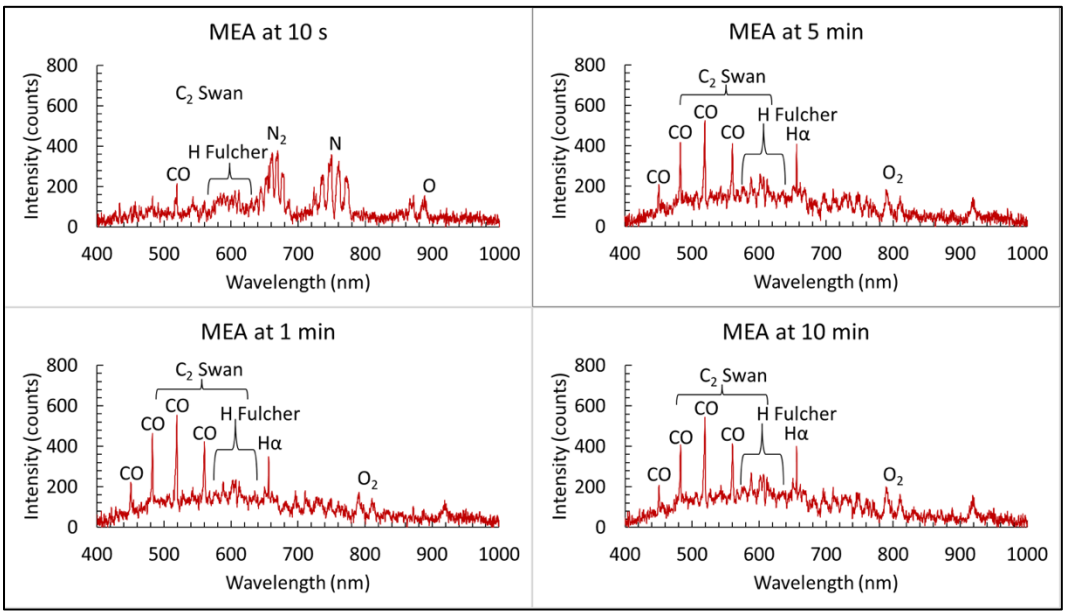

Figure 1. Shown are optical emission spectra of various MEA plasmas as an evolution in time. The time points of 10 s, 1 min, 5 min, and 10 min are shown in the top left, top right, bottom left and bottom right, respectively.

10.1002/asia.202400796

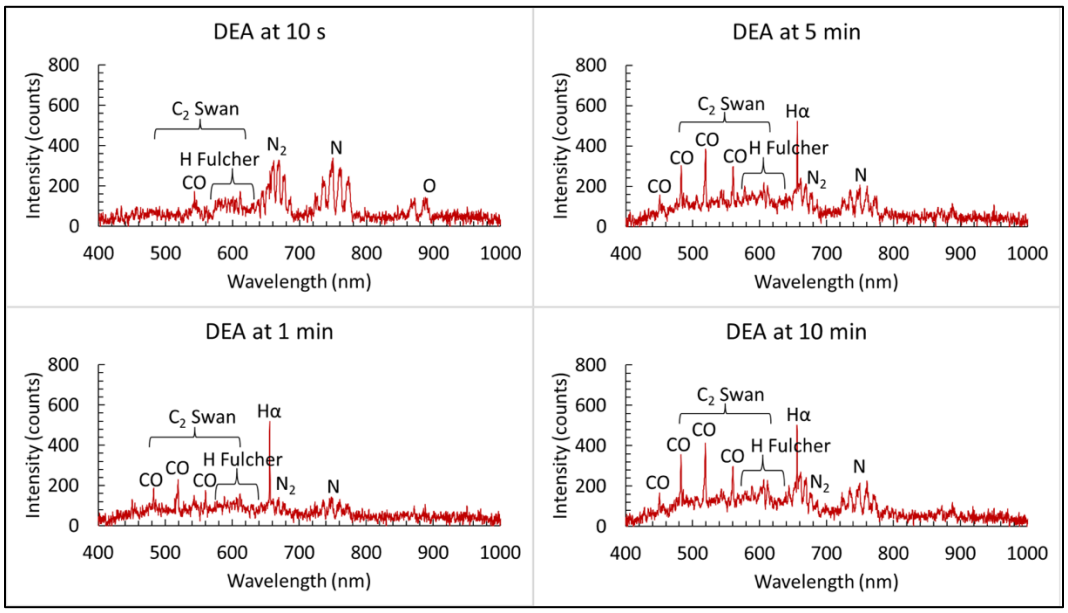

Figure 2. Shown are optical emission spectra of various DEA plasmas as an evolution in time. The time points of 10 s, 1 min, 5 min, and 10 min are shown in the top left, top right, bottom left and bottom right, respectively.

10.1002/asia.202400796

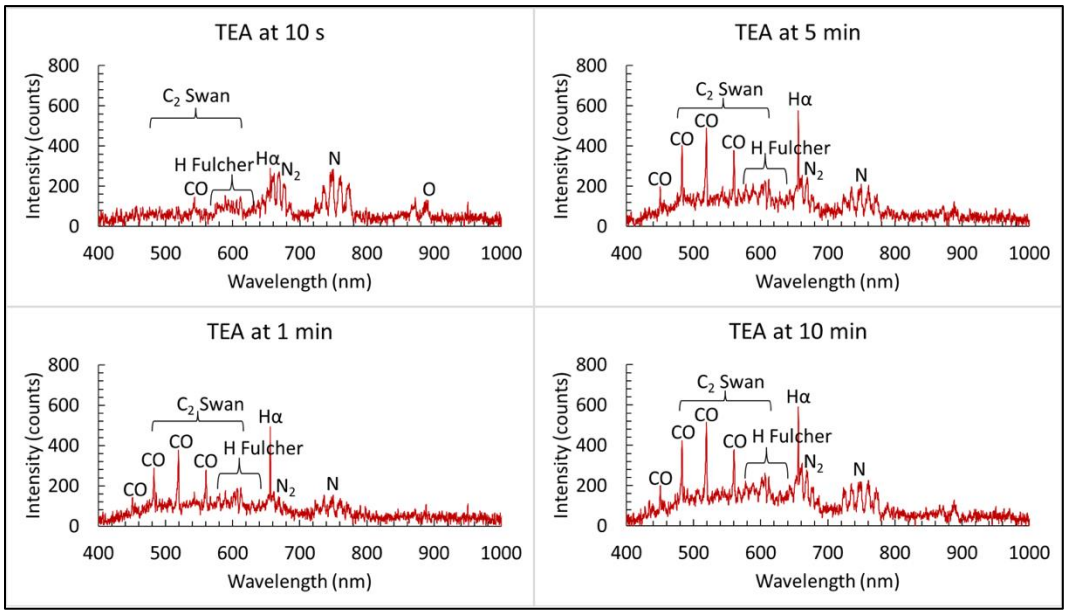

Figure 3. Shown are optical emission spectra of various TEA plasmas as an evolution in time. The time points of 10 s, 1 min, 5 min, and 10 min are shown in the top left, top right, bottom left and bottom right, respectively.

10.1002/asia.202400796

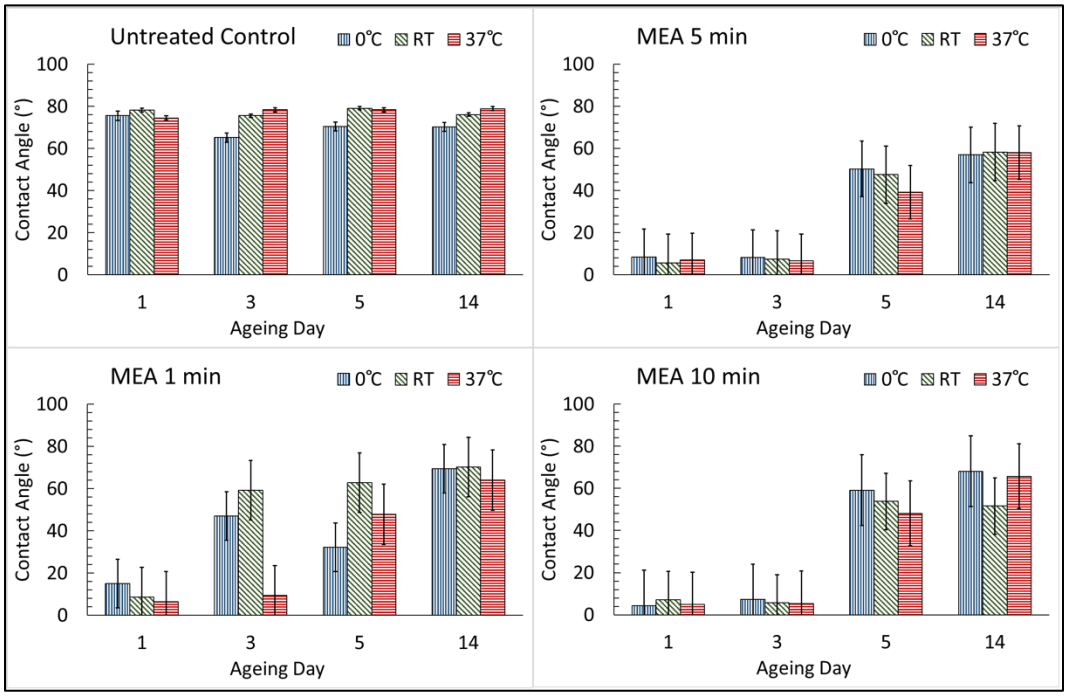

Figure 4. Shown are compiled contact angle data of various MEA-LTP treated samples as an evolution in time and temperature as well as the control in the top left, which is untreated. The time points of 10 s, 1 min, 5 min, and 10 min are shown in the top left, top right, bottom left and bottom right, respectively, and are the various LTP treatment times. Within the graphs are ageing times of 1, 3, 5, and 14 days. Bars are the standard error for 5 samples yielding 2 measurements each for n=10 per group and the values plotted are the numerical average.

10.1002/asia.202400796

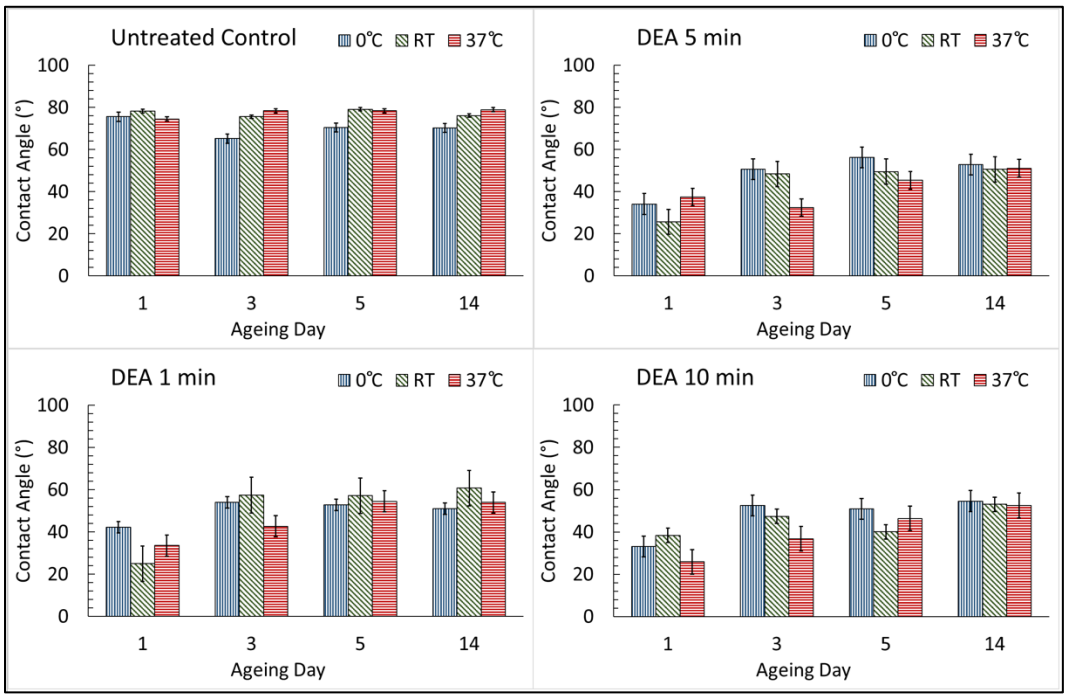

Figure 5. Shown are compiled contact angle data of various DEA-LTP treated samples as an evolution in time and temperature as well as the control in the top left, which is untreated. The time points of 10 s, 1 min, 5 min, and 10 min are shown in the top left, top right, bottom left and bottom right, respectively, and are the various LTP treatment times. Within the graphs are ageing times of 1, 3, 5, and 14 days. Bars are the standard error for 5 samples yielding 2 measurements each for n=10 per group and the values plotted are the numerical average.

10.1002/asia.202400796

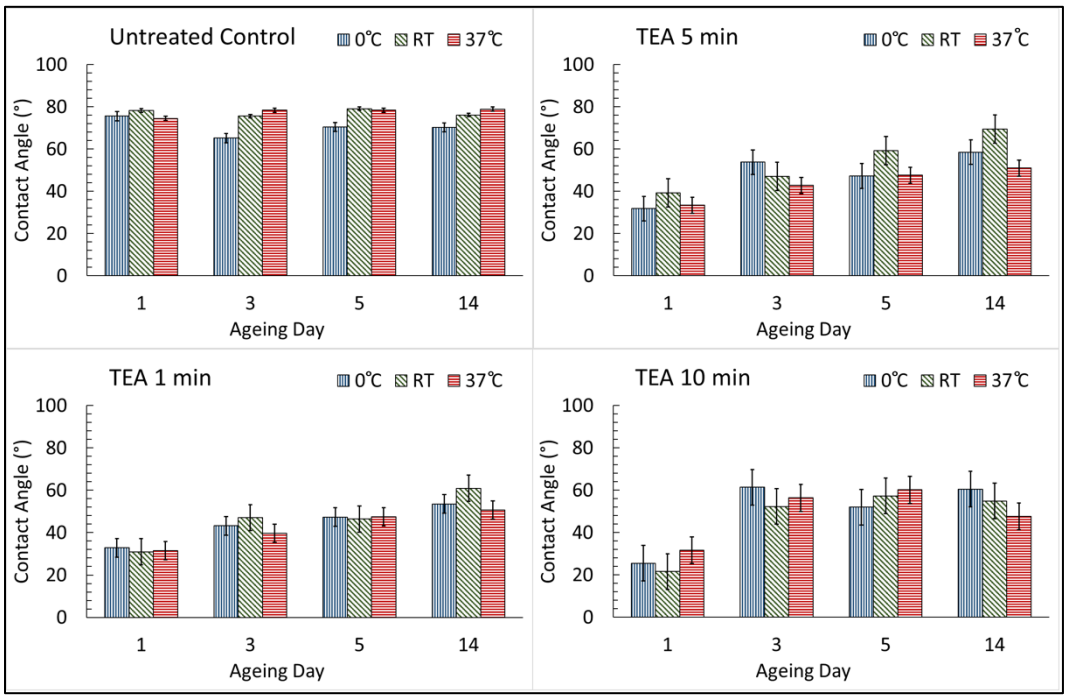

Figure 6. Shown are compiled contact angle data of various TEA-LTP treated samples as an evolution in time and temperature as well as the control in the top left, which is untreated. The time points of 10 s, 1 min, 5 min, and 10 min are shown in the top left, top right, bottom left and bottom right, respectively, and are the various LTP treatment times. Within the graphs are ageing times of 1, 3, 5, and 14 days. Bars are the standard error for 5 samples yielding 2 measurements each for n=10 per group and the values plotted are the numerical average.

10.1002/asia.202400796

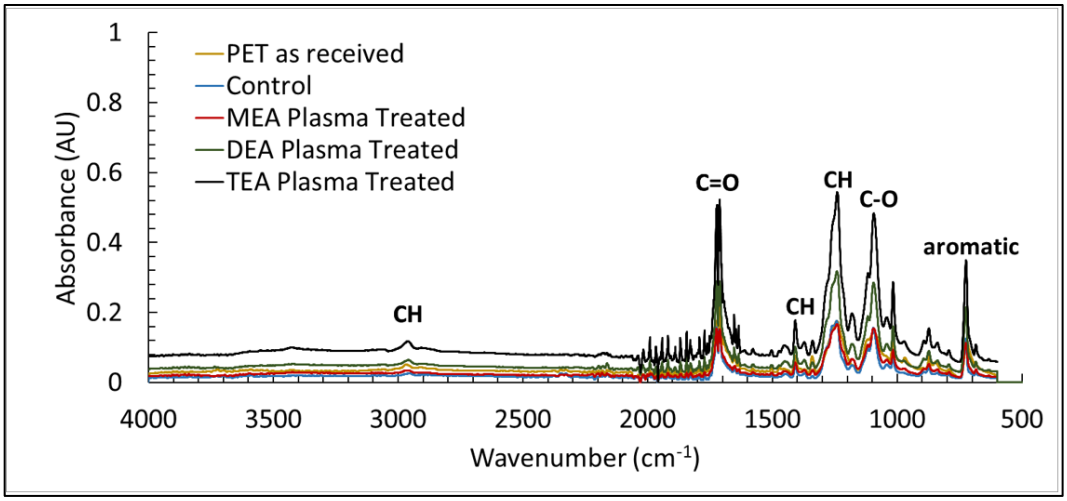

Figure 7. Show are overlaid FTIR spectra of the PET as received with the untreated control fibers and the LTP treated fibers with the MEA, DEA, and TEA LTP.

10.1002/asia.202400796

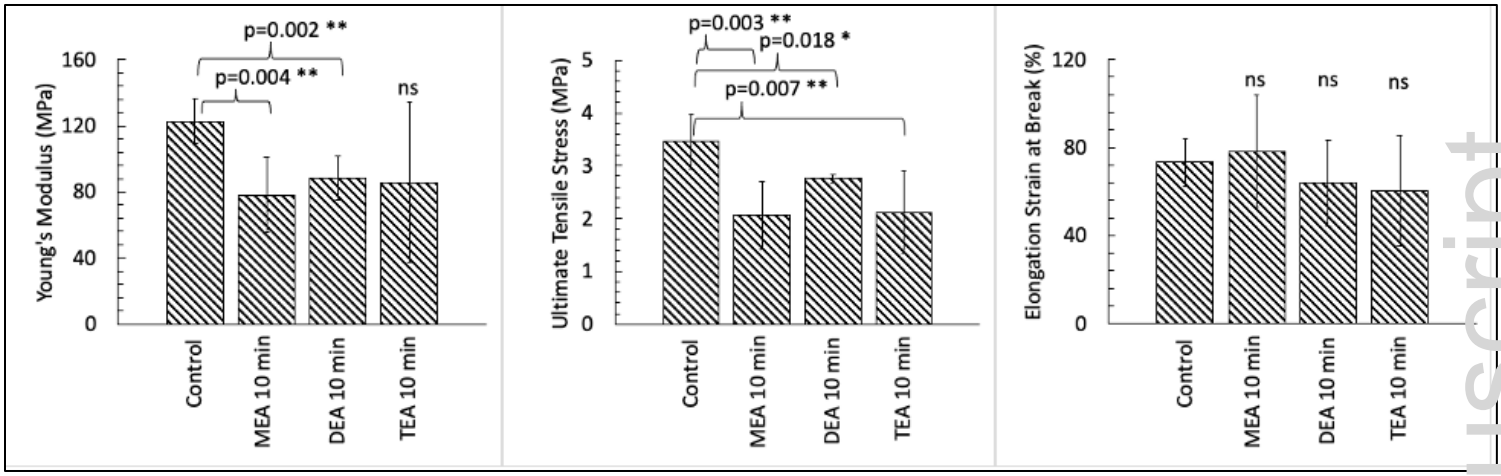

Figure 8. Compiled mechanical data from tensile tests for Young's Modulus, Ultimate Tensile Stress, and Elongation at Break for the control and LTP treated fiber samples. The bars are 1 standard deviation calculated from the best 5 samples per group of n=10 and the values are the numerical average. The statistical comparisons are from calculated Student's T-Test with 1 tail, unpaired, and assumed unequal variance.

10.1002/asia.202400796

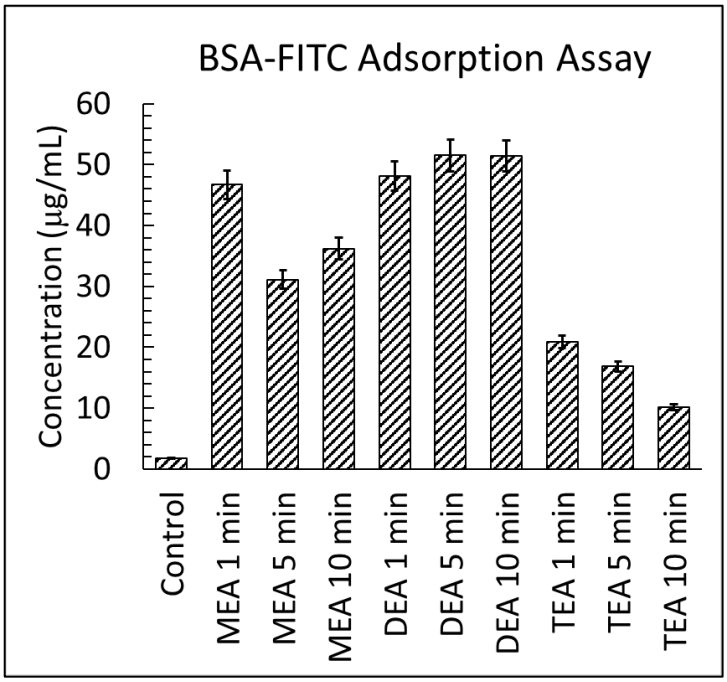

Figure 9. BSA-FITC adsorption tests comparing the untreated controls to the various MEA, DEA and TEA LTP treated samples for 1, 5, and 10 min exposure times. The bars are the standard error from at least 100 - 150 separate pixel measurements from triplet group trials of the fluorescent analysis in ImageJ. The values are the numerical average.

10.1002/asia.202400796

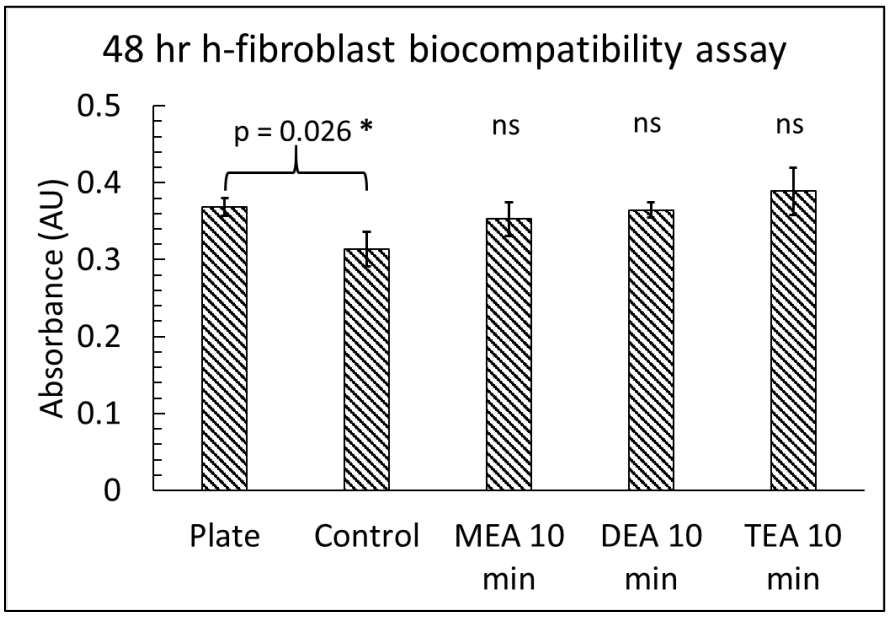

Figure 10. Compiled data from the fibroblast biocompatibility assay comparing the growth after 48 h on the culture plate, the control fibers, and the LTP treated fibers with MEA, DEA, and TEA all at the 10 min plasma exposure time point. The bars are 1 standard deviation calculated from the best triplicate samples for each group and the value is the numerical average. The statistical comparison is from Student's T-Test with 1 tail, unpaired, and assumed unequal variance.

10.1002/asia.202400796

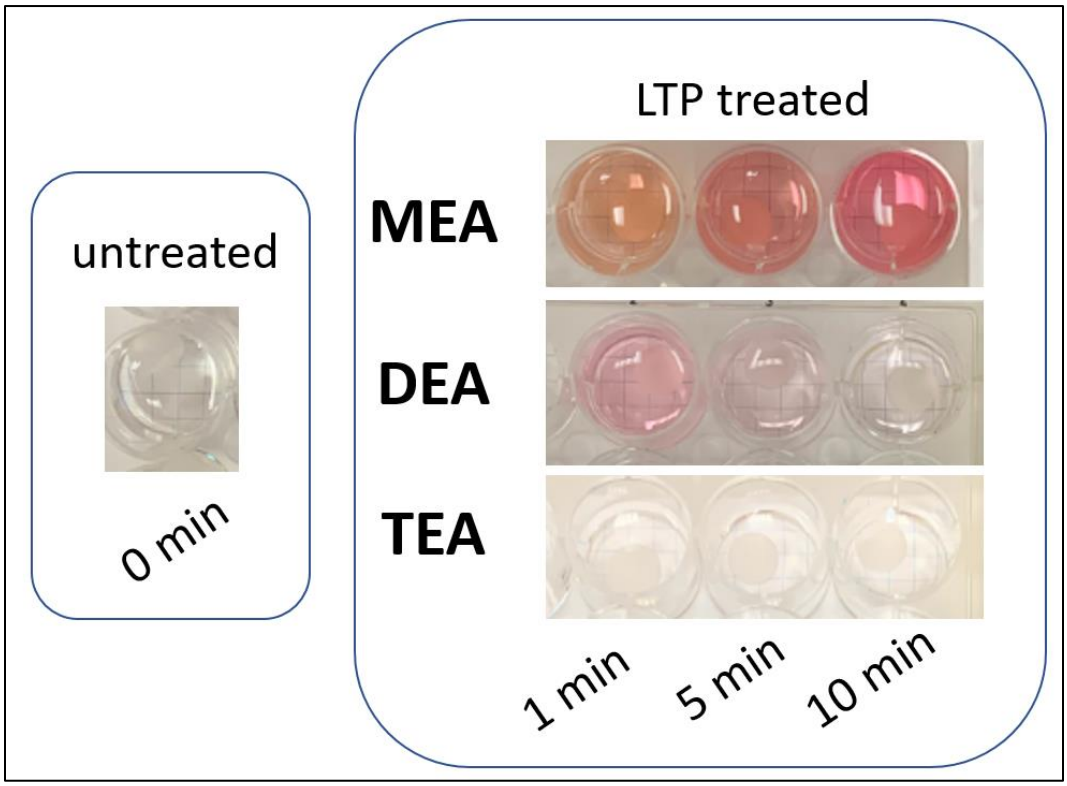

Figure 11. Spot test for NO release using the Griess assay. The comparisons of untreated control vs. 1 min, 5 min, and 10 min LTP exposure times for MEA, DEA and TEA are shown. The orange color in the MEA 1 min could be accounted for by undesirable side products.

10.1002/asia.202400796

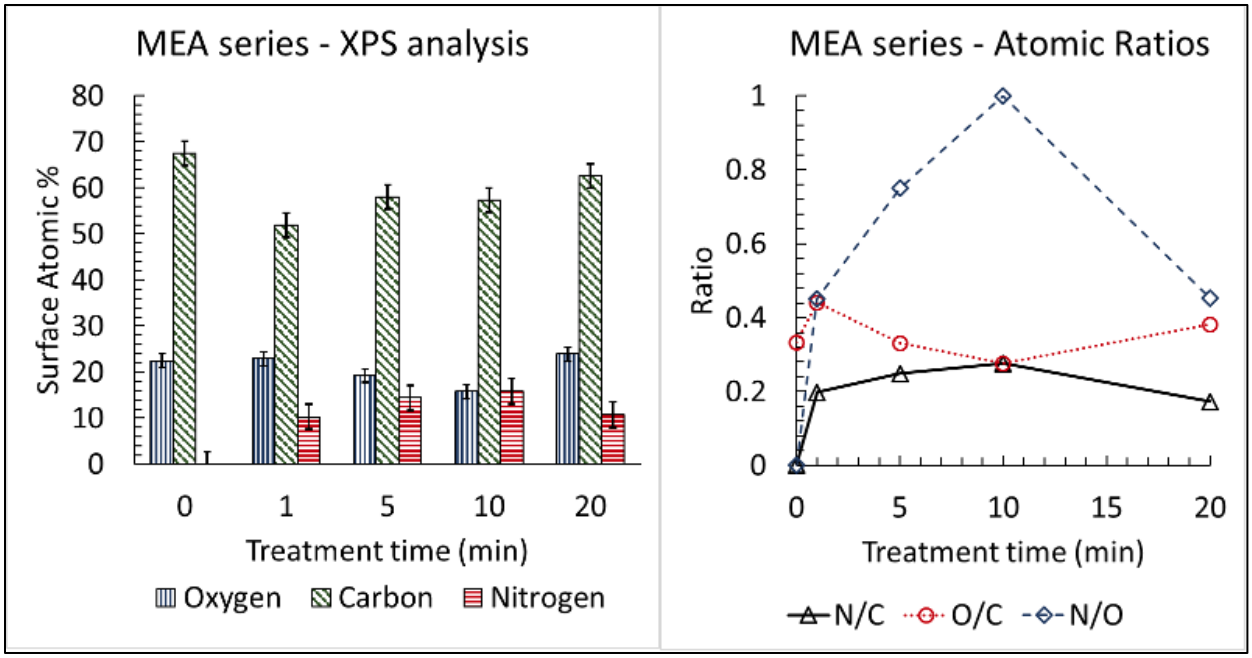

Figure 12. XPS analysis for the surface are shown in the graph on the left for the various conditions where 0 min is the untreated PET fiber mats and the 1, 5, 10, and 20 min are the LTP exposure times for MEA plasmas. The bars are 1 standard deviation for 3 surface measurements and the surface atomic percent for oxygen, carbon, and nitrogen are shown. The graph on the right are the plotted ratios of the various elements.

10.1002/asia.202400796

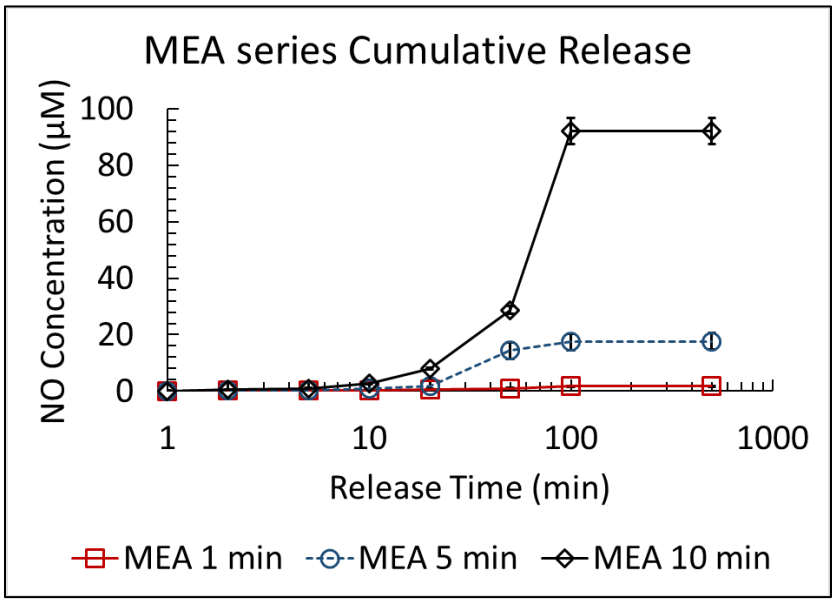

Figure 13. Cumulative release profiles for the MEA-LTP treated fiber samples are shown as a function of time. The measurements are numerical averages of triplicates for each time point and the bars are the standard error. The control is omitted since it did not have a detectable signal.

10.1002/asia.202400796

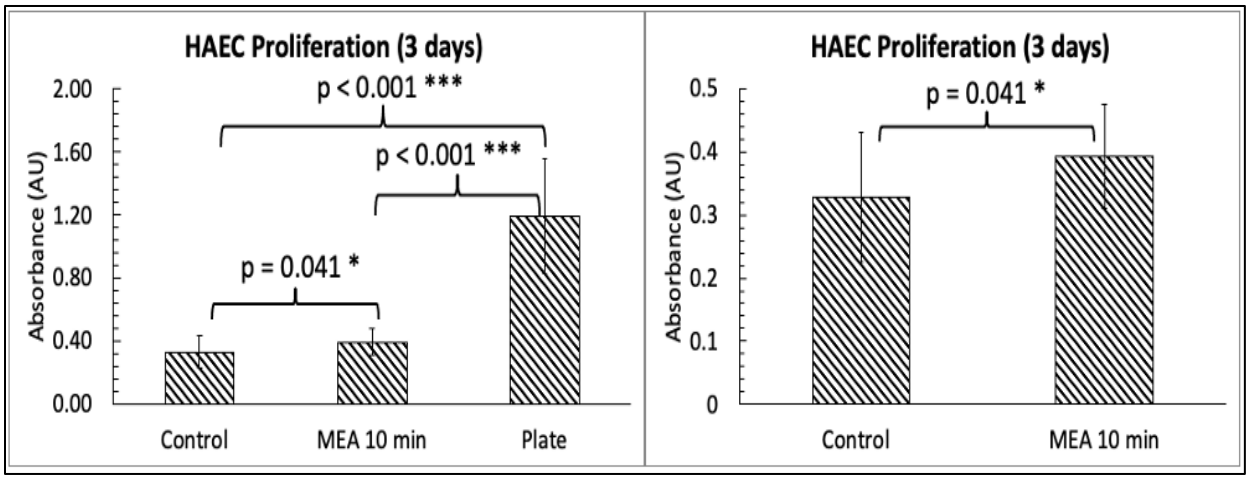

Figure 14. The results of the MTS assay of the endothelial cell study are shown. The bars are 1 standard deviation for the best 4 measurements of n=5 samples. The large amount of noise still yielded stastistical differences using Student's T-Test with 1 tail, unpaired, and assumed unequal variance.

10.1002/asia.202400796

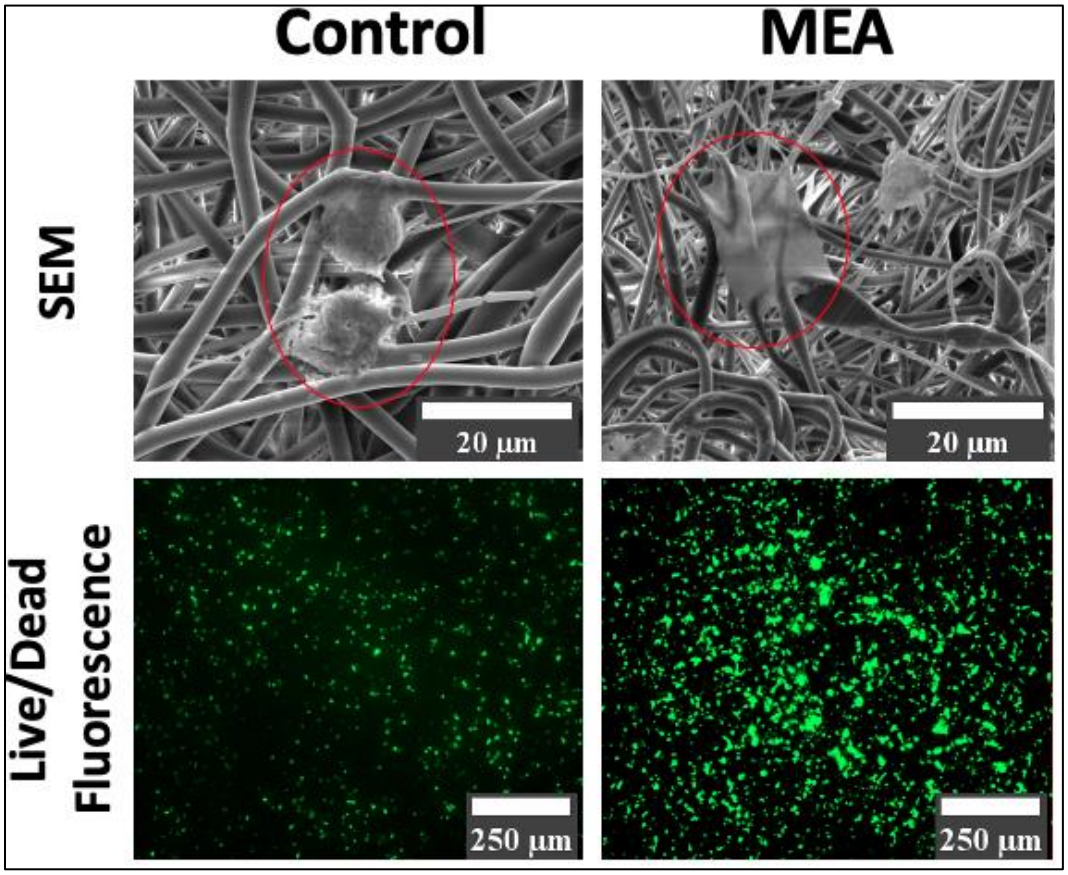

Figure 15. SEM micrographs of the control fibers with cells and the MEA treated fibers with cells are shown in the top panels. Live/dead fluorescence images of the same conditions are shown in the bottom panels with green channel live and dead channel red. Note that the field is flooded with green signals. And almost no visible red signals. In the SEM micrographs red circles are used to indicate the cells.

10.1002/asia.202400796

Table 1. DSC analysis is summarized in the following and includes the measured glass transition, cold crystallization peak temperature and enthalpy, and the melt peak and enthalpy.

DSC Analysis					
Sample	**Glass Transition (°C)**	**Cold Crystallization Peak (°C)**	**Cold Crystallization Enthalpy (J/g)**	**Melt Peak (°C)**	**Melt Enthalpy (J/g)**
Control	60.5	126.80	16.45	251.99	28.33
MEA 10 min	63.32	127.92	18.52	252.60	32.34
DEA 10 min	49.14	130.38	20.90	251.88	27.79
DEA 10 min	46.34	130.48	20.23	251.44	34.57